X-ray Computed Tomography and Numerical Analysis of Water-saturated Porous Materials

Master's Thesis

Heli Siltanen
University of Jyväskylä,
Department of Physics

September 3, 2012

Preface

I want to pay special regard for my instructors, professor Markku Kataja and PhD Viivi Koivu, who entrusted me this intriguing subject of research and thesis. Thank you for your indefinite patience and constructive advice. Thanks also to Tuomas Turpeinen who alongside Markku inspected my thesis.

I also wish to thank all the wonderful people in the tomography group who encouraged and counseled me during the experimental part of my work. Thank you, Tuomas as well as Markko Myllys, for our discussions on x-ray computed tomography and your assistance in the XRadia lab. Thank you, Arttu Miettinen, for your support with IT and image processing.

Thank you, Jarno Alaraudanjoki, for your help with the permeability device. Thanks for your MatLab codes that served as a basis for the processing of permeability data. Thank you for your mental support and for sharing your knowledge with me.

Thank you, Einari Periainen, for making sample holders and preparing samples for my study. I won't forget how you tried to respond to all my wishes and offered some original ideas of your own.

Last but not least I want to thank my family. Thank you, my parents, for all the support during my studies. Thank you, my sister, and your family, for offering me a place to stay whenever I needed to get away.

Thank you, Tuomo, for pushing me to make this happen. I will always love you for everything that you are. No one could ever replace you.

Abstract

A porous material consists of the solid part and the pore space filled with ambient fluid. The knowlegde of the properties of flow through porous media is essential in many fields of science and technology. Permeability of a porous medium is a material parameter that is often needed. Permeability can be determined experimentally using the Darcy's law which states that pressure gradient and flow velocity are proportional.

When air or another gas and water have been used to measure permeability, it has been observed that the permeability for water is lower although it should depend merely on the material. One of the possible explanations is the Klinkenberg effect which happens when the mean free path of the gas molecule becomes significant with respect to the pore diameter. In this case the gas molecules have non-zero flow speed on the solid surface. Another explanation that has to be considered are the structural changes of the porous material due to water absorption.

In recent years x-ray computed tomography has been a successful method in determining the permeability of a dry porous material numerically. Using this method a three-dimensional picture of the sample structure can be reconstructed from consequent traditional radiographs. By tresholding a greyscale image into a binary image and applying the Lattice Boltzmann method the flow field through the sample can be simulated.

The goal of this work is to develop a method of imaging a water-saturated porous material with x-ray tomography so that flow through that material can be studied numerically. There are, however, particular challenges when tomographic images are taken of a wet sample, especially gaining sufficient contrast between solid and liquid phases. Things that have to be taken into account doing this are covered in this work.

In this work an explanation for the difference in permeability values measured for air and water is also seeked. For this purpose the same sample was imaged dry and wet and an effort was made to crop the same physical part of the sample for numerical calculations. For comparison, the experimental values of permeability for air and water were determined.

Both the experimental and numerical results for each material were similar, although their actual values differed a little. The outcome confirms that the swelling of a porous material in water environment affects significantly on its permeability. In this respect, the work was succeeded.

Tiivistelmä

Huokoinen aine koostuu kiinteästä osasta ja kaasun tai nesteen täyttämästä huokostilavuudesta. Huokoisten aineiden läpi tapahtuvien virtauksien ominaisuuksien tuntemusta tarvitaan useilla tieteen ja teollisuuden aloilla. Huokoisen aineen permeabiliteetti on eräs materiaaliparametri, josta ollaan usein kiinnostuneita. Permeabiliteetti määritetään kokeellisesti käyttämällä Darcyn lakia, jonka mukaan paine-ero ja virtausnopeus ovat suoraan verrannolliset.

Kun permeabiliteettimittauksissa on käytetty ilmaa tai muita kaasuja ja vettä, on havaittu, että permeabiliteetti vedelle on pienempi, vaikka sen pitäisi riippua vain aineesta, jonka läpi virtaus tapahtuu. Selitykseksi esitetään esimerkiksi nk. Klinkenbergin ilmiötä, joka esiintyy, kun kaasumolekyylin vapaa matka kasvaa merkittäväksi huokosen halkaisijaan verrattuna. Tällöin kaasumolekyylien nopeus kiinteän aineen rajapinnassa on nollasta poikkeava. Toinen varteenotettava selitys ovat rakennemuutokset, joita tapahtuu nesteen imeytyessä huokoiseen aineeseen.

Viime vuosina kuivan huokoisen aineen permeabiliteetti on pystytty määrittämään myös numeerisesti käyttämällä hyväksi röntgentomografiakuvausta. Tällä menetelmällä voidaan perättäisistä tavanomaisista röntgenkuvista rekonstruktioida kolmiulotteinen kuva näytteen rakenteesta. Kynnystämällä harmaasävykuva mustavalkoiseksi ja käyttämällä nk. hila-Boltzmann-menetelmää voidaan simuloida virtauskenttä näytteen läpi.

Tässä työssä tavoitteena on kehittää menetelmä, jolla kuvata vesiympäristössä oleva huokoinen aine käyttäen röntgentomografiaa siten, että aineen läpi tapahtuvaa virtausta voidaan tarkastella numeerisesti. Märän huokoisen aineen tomografiakuvaukseen liittyy kuitenkin omat haasteensa, erityisesti kiinteän ja nestefaasin välisen kontrastin riittävyys. Työssä pyritään selvittämään, mitä seikkoja tulee ottaa huomioon.

Työssä etsitään myös selitystä ilmalle ja vedelle mitatun permeabiliteetin erolle. Tätä silmällä pitäen sama näyte kuvattiin kuivana ja vesiympäristössä, ja tomografiakuvista pyrittiin rajaamaan fyysisesti sama osa numeerista laskentaa varten. Vertailun vuoksi näytemateriaaleille määritettiin permeabiliteetin arvot kokeellisesti virtauttamalla niiden läpi ilmaa ja vettä.

Sekä kokeelliset että numeeriset tulokset eri materiaaleille ovat samansuuntaisia, vaikkakin ne poikkesivat toisistaan jonkin verran. Tulokset vahvistavat, että huokoisen materiaalin turpoaminen vedessä vaikuttaa merkittävästi sen permeabiliteetin arvoon. Työ onnistui siis tarkoituksessaan.

Contents

1 Introduction

In many fields of science and technology such as soil science and papermaking industry, knowledge of porous materials involved is essential. Paper processing involves the use of wet pressing felt and water removal from the cellulose [1]. The structure and fluid flow properties of these materials are of great importance.

A porous medium consists of solid material eg. in the form of grains or fibres, and pore or void space inbetween. The pore space is most often filled with air, water or both. Porous materials allow fluids flow through them. The efficiency of the fluid flow through a porous medium is quantified by permeability. According to the experimental law of Darcy the flow velocity is proportional to the pressure gradient [2]. Darcy's law is the basis for measuring permeability that is defined by means of the proportionality coefficient between pressure gradient and flow velocity.

In some special cases with simplified flow geometry such as a bed of identical spheres or cylinders, fluid flow can be solved analytically. Several formulas that include other material parameters give estimates for permeability. One or more of these parameters may have to be defined experimentally, which makes the equations semiempirical. [2]

Recently there has been attempts to solve the fluid flow numerically [3] [4]. The real geometry of the material is obtained using x-ray computed tomography. The sample is illuminated with x-rays that are partially absorbed and the scattered intensity distribution is observed by the detector. Shadowimages of the sample are taken from all around the sample and a 3D reconstruction of the structure is computed. The reconstructed image is filtered and converted into binary image.

Boltzmann equation is a differential equation from which the basic conservation laws of hydrodynamics can be derived. Solving the Boltzmann equation with selected boundary conditions for a binary matrix is called the Lattice Boltzmann method. Utilizing this numerical method gives the flow velocity field and flow parameters such as permeability. [5]

The use of the Lattice Boltzmann method sets some conditions for the tomographic image. The sample has to represent the material well enough eg. in terms of mass density and surface topography, the image must not suffer from remarkable noise and the contrast between solid material and pore space must be adequate. Within these limits this method has been shown to work in the case of dry samples of wet pressing felt, cardboard and paper. The reference was given by experiments. [4]

However, when fluid flow through the porous medium is of greatest interest, the material is typically not dry but in contact with water. The structure of many

porous materials changes when they absorb water and swell. Flow experiments show a discrepancy between permeability for air and water [6]. More accurate knowledge of the difference in structure and fluid flow properties of dry and wet porous material would be beneficial.

The measured difference between permeability for air and water might be explained if the same numerics could be run whether pore fluid is air or water. There are, however problems that arise when a wet sample is imaged. The most important of these are the deterioration of contrast, the possible instability of the sample and air pockets left inside the sample.

The main goal of this work is to develop a method for imaging porous materials in water environment using x-ray micro-CT so that the Lattice Boltzmann method could be successfully applied to solve fluid flow through them. The numerical permeability results are to be compared with the experimental values. One aim is to show the influence of structural changes in a material on its permeability.

The following section sheds some light on the background of this study. The characteristics of porous materials are described and Darcy's law is introduced. Deviations from Darcy's law and possible explanations for the difference in permeability for air and water are discussed. At the end of the section a summary of related studies is given.

Section 3 gives more information about x-ray computed tomography, the sample materials, sample preparation and imaging procedures. The experimental and numerical methods used in this work are outlined. Observations of the tomographic imaging of wet samples are also dealt with.

In section 4 the acquired tomographic images are studied. The ability to perform the same numerical procedures for matrices from tomographic images of dry and wet samples is under examination. The values of permeability obtained numerically and experimentally are compared. The expected difference in experimental values of permeability for air and water is discussed and compared with the difference in numerical values of dry and wet samples.

Section 5 gives an overall picture of how the tomographic imaging of materials in water environment and the numerical analysis succeeded in this work. It explains what problems arised as well as possible reasons and solutions for these difficulties. The future prospects of imaging water-swollen samples more carefully are pondered and some subjects for further study are proposed.

2 Theoretical and experimental background

2.1 Porous materials

Everyday examples of porous materials are numerous. Some well-known examples are filter paper, wood and fabrics. Porous materials differ in many respects but they all have some features in common. (See figure 1.)

Jacob Bear [6, p. 14] states three essential characteristics that describe a porous medium.

1. Porous materials are multiphase materials that consist of solid matrix, eg. grains or fibres, and the void, or pore space between. The pore space is filled with a fluid or several fluids. At least one of the phases included in the material is not solid.
2. The specific surface of the porous material is relatively high. In other words, the solid matrix extends throughout the medium. In addition, the openings in the pore volume are quite narrow.
3. There must be connections between the pores, so that continuous paths from the other side of the porous medium to the other are formed. This is crucial for fluid flow through the medium. The interconnected pores form the effective pore space.

Porous media and especially the fluid flows through them play an important role in such fields in the modern society as papermaking and the final placing of nuclear waste.

2.1.1 *Properties of porous media*

A usual statistical quantity used in association with porous materials is porosity ϕ, the proportion of void volume to bulk volume. Another, often more useful in terms of flow through a porous medium is effective porosity ϕ_e, the proportion of interconnected or effective pore volume to bulk volume. [6, p. 43–44] The permeability of a porous medium, that is the proportionality factor between the flow velocity and the pressure drop across the medium, has a strong dependence on its porosity.

A statistical approach is needed to describe the pore space when the material is consolidated and the particle size distribution cannot be obtained. A pore-size distribution [6, p. 41] can be defined for example in terms of pore diameter δ, the diameter of the largest sphere that contains the point at which δ is determined and is totally included in pore space. The fraction α of the total amount of these

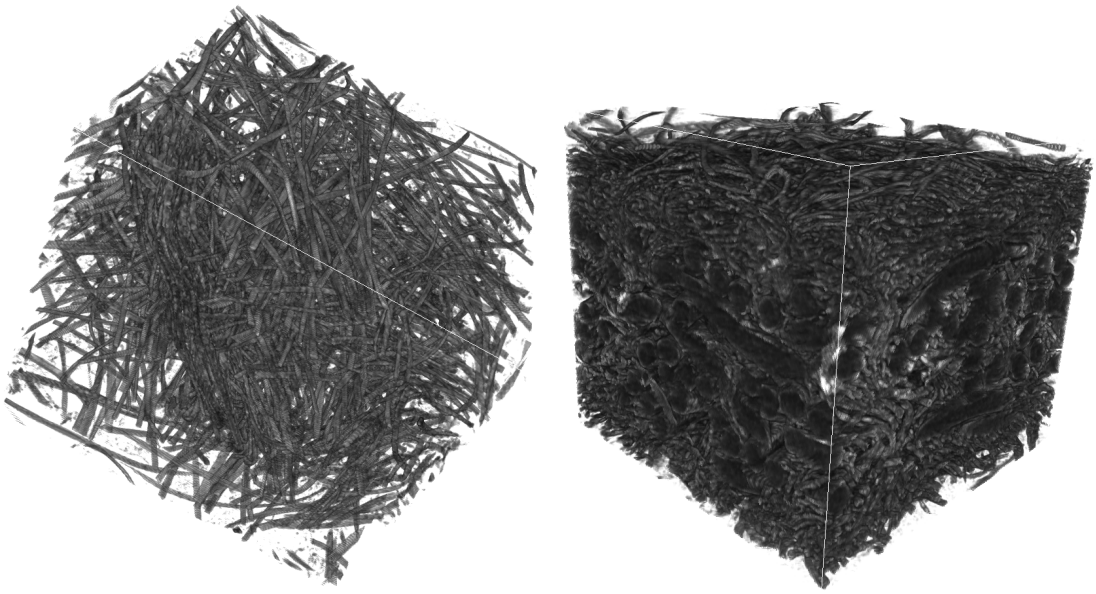

Figure 1: Visualisations of the 3D structure of dry synthetic chammy (on the left) and press felt.

spheres have a diameter between δ and $\delta + \mathrm{d}\delta$. An integral over all pore-sizes gives

$$\int_0^\infty \alpha(\delta)\mathrm{d}\delta = 1. \tag{1}$$

Another useful concept is the specific surface of a porous medium. Specific surface is defined as the interstitial area of the pore volume with respect to bulk volume. The specific surface is determined by the shape and size of the grains of fibres, the porosity and the packing. [6, p. 50, 51] The specific surface has a significant effect on the flow through a porous medium because it affects its permeability, though not as much as porosity.

2.1.2 *Permeability and Darcy's law*

Let us consider flow through a porous medium when the continuum approach is valid, i.e. the mean free path of a fluid particle is much smaller than the specific length scale of the porous material. In this flow region the flow velocity through the porous medium is proportional to the pressure gradient across the medium. The proportionality coeffient gives the permeability of the medium according to Darcy's law [2, p. 157]

$$\vec{v} = -\frac{k}{\mu}\nabla p, \tag{2}$$

where $\vec{v}$ is the flow velocity, k is the permeability coefficient, μ is the viscosity of the fluid and ∇p is the pressure gradient. In a general case permeability is a tensor quantity.

Let us now discuss a simple case of one-dimensional incompressible flow through a sample of thickness L in the direction of the main flow and cross-sectional area A normal to the flow. In this case Darcy's law [6, p. 120, 121] becomes

$$\begin{aligned} Q &= A\frac{k}{\mu}\frac{\Delta p}{L} \\ \Leftrightarrow k &= \frac{\mu L}{A}\frac{Q}{\Delta p} \end{aligned} \tag{3}$$

where Δp is the pressure drop between inlet and outlet and k is the permeability coefficient, the SI unit of which is $[k] = \mathrm{m}^2$.

The permeability obtained from equation 3 is valid for incompressible flow, eg. water flow. When gas flow is considered, the compressibility of the flow has to be taken into account. For isothermal compressible gas flow pQ is constant because pV is constant. Thus, if pressure and volumetric flow rate are measured for example at the outlet, it holds that

$$p_{\mathrm{out}}Q_{\mathrm{out}} = pQ = k_g A\frac{p_{\mathrm{ave}}}{\mu}\frac{\Delta p}{L} \tag{4}$$

or, in terms of permeability

$$k_g = \frac{\mu L}{A}\frac{p_{\mathrm{out}}}{p_{\mathrm{ave}}}\frac{Q_{\mathrm{out}}}{\Delta p}, \tag{5}$$

where p_{out} and Q_{out} are the pressure and volumetric flow rate readings at the outlet, k_g is the permeability for gas and p_{ave} is the mean pore pressure i.e. the arithmetic mean of the pressures at the inlet and the outlet. [7, p. 288]

Experiments have shown that permeability has a strong dependence on porosity. Several empirical and semi-empirical laws for this purpose have been developed. Kozeny and Carman obtained a useful equation applicable to a variety of materials although some assumptions on the flow geometry must be made in its derivation. According to Kozeny-Carman equation in it's usual form [6, p. 111] [2, p. 170, 171]

$$k_{KC} = \frac{\phi^3}{C\tau^2\left(1-\phi\right)^2 S_0^2} \tag{6}$$

where ϕ is porosity, C is a constant, τ is tortuosity and S_0 is the specific surface. The Kozeny-Carman permeability increases rapidly with increasing porosity, but

it decreases with increasing specific surface. However, one must bear in mind that usually a change in porosity has a straightforward effect on specific surface by the change in volume. [6, p. 51] Also the arrangement and the size distribution of flow capillaries affect the permeability. The Kozeny-Carman model is applicable to porosities $\phi < 0.95$. [2, p. 172]

2.2 The difference between permeability for water and air

As long as Darcy's law in equation 2 is valid, the permeability of a material should be a property of a material and independent of fluid. However, measurements often show a discrepancy between permeability for gases and liquids beyond experimental error. In many experiments values of permeability obtained for water are significantly lower than for gas especially for low permeable materials at low pore pressures. [8, p. 200] [6, p. 128] There are several possible explanations for these differences, for example the swelling of materials in water and flow phenomena specific for gases at low pressures in small capillaries.

2.2.1 *Wetting and swelling*

As permeability of a porous material is a function of its porosity and specific surface, it will be affected by structural changes in the material. Many porous materials allow water to penetrate into the pore space and in many fibrous materials, also inside the fibre walls. This causes swelling of fibres and the porous material as a whole. Thus the differences in permeability for air and water may be explained by swelling of the network and dimensional changes of pores and capillaries. [8, p. 200] [9, p. 153, 154, 156]

Swelling of processed pulp fibres has been a subject of research [10] [11]. Because majority of cellulosic materials are formed in an aqueous medium, the water-swollen state is their natural state. When water is introduced to dryed and calendered pulp, e.g. paper, the fibres tend to regain their original shape. The lumen may open up and the compressed fibre may become more tube-like in shape, depending on the pulp processing procedures. This results in cross-sectional swelling of fibres. Water absorption also enhances development of inter-fibre voids and pores in the paper structure. These two processes together contribute to the swelling of paper on wetting. [10] [11, p. 745]

2.2.2 *Klinkenberg effect*

As stated earlier, Darcy's law is valid in continuum approximation. This condition can be expressed in terms of scale parameters introducing the so called Knudsen

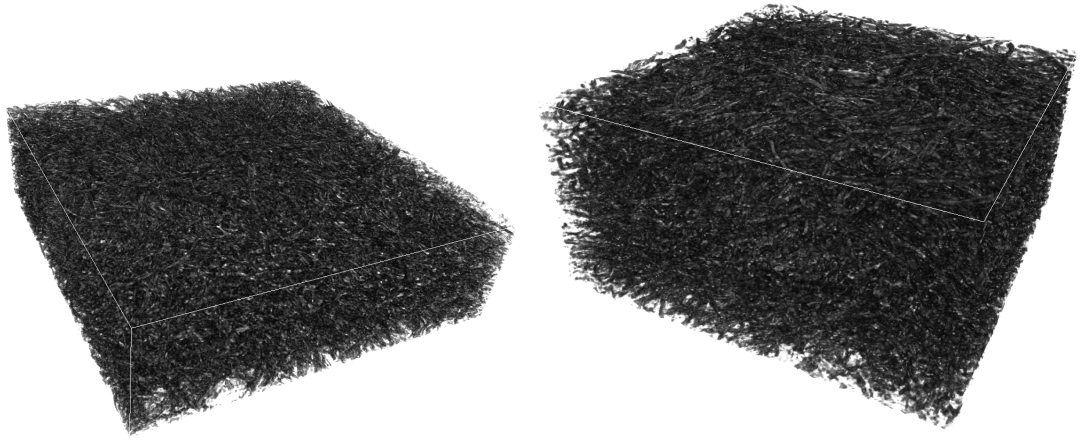

Figure 2: Visualisations of the 3D structure of dry (on the left) and wet cardboard.

number [12, p. 172] that is defined as the ratio of the mean free path λ of the gas molecule and the pore size l_p:

$$Kn = \frac{\lambda}{l_p}. \tag{7}$$

Different flow regimes can be separated by means of Knudsen number in the following way [13, p. 1]

$$\begin{cases} Kn < 0.001, \text{continuum flow} \\ 0.001 < Kn < 0.1, \text{slip flow} \\ 0.1 < Kn < 10, \text{transition flow} \\ Kn > 10, \text{free molecular flow.} \end{cases}$$

When the mean free path is negligible compared to the pore size, molecular effects can be ignored and the usual boundary condition of zero flow velocity on the pore walls is valid and Hagen-Poiseuille equation governing gas flow through capillaries can be applied to porous media. However, when Knudsen number approaches unity, collisions of gas molecules with pore walls become more and more significant and the collisions between gas molecules less important. This results in a non-zero average flow velocity in the vicinity of pore walls. In this flow region the fluid can no more be treated as continuum. This so called slip effect is especially significant in the case of low permeable media, where the pore size is usually very small, and at low pore pressures when the mean free path of gas molecules becomes longer. [8, p. 202] [12, p. 172]

Klinkenberg derived an equation for gas permeability in a porous medium assuming a non-zero flow velocity with respect to the wall. He first considered the case of

gas flow through a straight capillary and obtained a generalisation of Poiseuille's equation with a slip term dependent on the ratio of the mean free path of gas molecules and the capillary radius. He then applied this approach to a porous medium with equally sized and randomly oriented capillaries and used Darcy's law to obtain an equation for permeability as a function of mean free path or average pressure. Klinkenberg equation is

$$k_g = k_l \left(1 + \frac{b}{\bar{p}}\right) = k_l \left(1 + \frac{4c\lambda}{r}\right), \tag{8}$$

where k_g is the apparent gas permeability, k_l is the liquid permeability, b is the Klinkenberg factor, $\bar{p}$ is the mean pore pressure, that is arithmetic mean of the inlet and outlet pressures of the sample, c is a constant, λ is the mean free path and r is the capillary (or pore) radius. [8, p. 203]

From equation 8 it follows that gas permeability increases linearly with increasing reciprocal mean pressure. A plot of permeability against reciprocal mean pore pressure extrapolated to infinite pressure should thus give the true permeability, the permeability for liquid. In addition, as long as the mean pore pressure remains constant, gas permeability is independent of the pressure difference. Also, the permeability for different gases is different at the same mean pressure, because they have different values of mean free path λ. [8, p. 204]

The Klinkenberg factor b depends on the pore structure and temperature. The Klinkenberg effect becomes less significant as the permeability increases, as the permeability is proportional to inverse pore radius. The dependence of b on liquid permeability k_l can be expressed as a power law

$$b \propto k_l^{-C}, \tag{9}$$

where C is a positive constant having an experimental value 0.36. In addition, b increases with increasing pressure. [8, p. 204] [14, p. 1315, 1324] [15, p. 120]

2.3 Earlier experiments concerning the difference between gas and liquid permeability

2.3.1 *Klinkenberg's experiments*

Klinkenberg carried out several measurements to prove his statements concerning gas flow in porous media [8]. The samples he used are four Jena glass filters with true permeability ranging approximately from 0,2–8,5 $\cdot 10^{-11}$ m^2 and eight core samples with true permeability values of 0,02–1,33 $\cdot 10^{-9}$ m^2. Air permeability was measured for these samples at different pore pressures, varying from about 0.01

up to 20 atmospheres. The results showed approximately linear relations between the apparent permeability and the reciprocal mean pressure for each sample with different b values. The parameter b decreased with increasing permeability. To be more exact, b was not constant but a function of pressure and was shown to increase with increasing pore pressure. [8, p. 204–206]

In addition, permeability measurements with nitrogen, carbon dioxide and hydrogen were carried out in order to verify the fact that when the slip effect is high, permeability varies for different gases according to their mean free paths (see equation 8). Also, when compared at pressures when the mean free path was the same for different gases, the permeability should be the same as well. Both the requirements were met by the experimental results. [8, p. 204, 205]

When the apparent permeability for the previous samples and for eight more core samples was extrapolated to infinite pore pressure and compared with the liquid permeability measured with isooctane, it was observed that the results were in good agreement. This proves the fact that the gas permeability equals with the liquid permeability in the limit of infinite pressure.

2.3.2 *Nitrogen and water permeability in porous sedimentary rocks*

Tanikawa and Shimamoto studied gas and liquid permeability of some porous sedimentary rocks in attempt to verify the Klinkenberg effect quantitatively [14]. Permeability measurements for nitrogen gas and distilled water were run. Pressure cycle tests for nitrogen were carried out in such a way that the differential pore pressure was kept constant during the cycle and the flow rate at the downstream was controlled. The mean pore pressure was cycled from 5 to 160 MPa. The cycle was repeated with four or five values of differential pore pressure. [14, p. 1316, 1321]

Comparing the values of permeability for nitrogen and water for different samples, it was discovered that permeability for nitrogen gas was several times larger than for water for all the samples and the difference was larger for less permeable samples. It was shown that the gas permeability increases with increasing pore pressure. Results also implied that the difference between nitrogen and water permeability was largest for least permeable specimens. [14, p. 1322]

When the nitrogen permeability at the same average pore pressure was studied, it was observed to increase with increasing differential pressure, which was in contradiction with Klinkenberg's theory. When the nitrogen permeability was plotted against the reciprocal mean pore pressure, a linear relationship in concordance with the Klinkenberg equation 8 was found in most cases. The liquid permeability estimated from the extrapolation to infinite pressure was lower than the actual measured water permeability for three samples, but the difference was much smaller

than the one between values of nitrogen and water permeability. [14, p. 1322, 1323]

In the study it was claimed that the Klinkenberg effect is significant when the permeability is lower than 10^{-18} m^2. The conclusion was based on the experimental power law relationship found between the parameter b and liquid permeability. The plot of ratio of nitrogen and water permeability against the differential pore pressure for different liquid permeability showed clearly that the Klinkenberg effect was significant only at low pore pressures and low values of permeability. [14, p. 1316, 1323, 1324, 1337]

2.3.3 *Solutions for steady-state and transient gas flow in porous media*

Wu, Pruess and Persoff introduced in their paper a new pressure variable and derived a governing equation for gas flow through a porous medium with Klinkenberg effects [15]. They derived analytical solutions for steady-state and transient flow. They examined the accuracy of the numerical simulation scheme TOUGH2 with real life parameters from a tuff formation. The numerical results for both the steady-state and transient flow were in good agreement with the analytical solutions. [15, p. 127, 128]

Steady-state gas flow was also tested experimentally for two rock core samples to evaluate liquid permeability and Klinkenberg factor b. The collected data was studied using the traditional Klinkenberg method and the developed exact Klinkenberg analysis derived from the exact steady-state flow solution. The two methods give parameters quite close to each other but the traditional method seemed to have better correlation. [15, p.131, 132]

2.3.4 *Comparison of water and argon permeability in natural clay-bearing fault gouge*

Faulkner and Rutter determined the permeability for argon gas and water of clay-bearing fault rock samples in order to identify some potential physicochemical interactions between rock and pore fluid [16]. The samples characteristics were studied to estimate how likely some of these interactions were to occur. The samples had a bimodal grain size distribution, the grain size < 2 μm being dominant. The porosity of the samples varied from 12 to 27 % before pressurisation and from 2 to 5 % after depressurisation of samples that had been subjected to high pressure. The fraction of swelling phases in the samples was concluded to be much lower than 1 %. [16, p. 16; 415–417]

Measurements with first argon and then water as pore fluid were carried out at confining pressures ranging up to 200 MPa at 20 °C and a pore pressure of 40 MPa.

Values of permeability from 10^{-17} down to 10^{-21} m^2 were measured. The results indicated a reduction in permeability of approximately one order of magnitude with introduction of water. The authors discussed the possibility of a few explanations for the observed behaviour. [16, p. 16; 417, 418]

It was concluded that the Klinkenberg effect was not significant as the ratio of the mean free path of argon and the mean pore radius is negligible. The authors also deduced that any argon pockets remained within the sample on the change of pore fluid into water occupied such a small volume of the pore space that the water permeability was not affected distinctly. The existence of swelling phases would have decreased the water permeability of the samples, but their absence was shown by x-ray diffraction tests. Enhanced compaction of the gouge due to introduction of water would have had the same effect, but no such phenomenon was observed in the measurements. [16, p. 16; 421, 422]

The apparent reduction of permeability may, however, be explained by thin layers of structured water on mineral surfaces of the rock. The information about the rock samples indicates that the pore apertures are small enough to allow interaction between these adsorbed layers. This reduces the effective pore size and, consequently, the permeability. The structured water layers are concluded to be the best explanation for the difference between the values of argon and water permeability in this study. [16, p. 16; 422, 423]

3 Experimental and numerical methods

3.1 X-ray microcomputed tomography

X-ray tomography is a nonintrusive method for studying true three-dimensional structure of materials. It is based on the same principle as the traditional x-ray imaging but instead of one or a few two-dimensional radiographs x-ray computed tomography, or CT, provides a complete 3D reconstruction of the original structure of the sample (see figure 3). In this study the reconstructed tomographic images are analysed numerically in order to determine some material parameters and the values of permeability of the materials are computed from flow simulations with the lattice Boltzmann method.

3.1.1 *Generation of x-rays*

X-rays are electromagnetic radiation with a wavelength range of 10–0.01 nm corresponding to an energy range of 120 eV–120 keV. X-rays can be generated e.g. in a classical x-ray tube where electrons are accelerated from a filament onto a metal target with high voltage. The collision gives rise to two types of x-radiation, braking radiation that is caused by the deceleration of electrons and characteristic radiation at energy levels when target atoms can be excited. An x-ray tube provides a continuous energy spectrum of polychromatic x-rays and relatively low intensity. A more effective way to generate x-rays is a synchrotron ring where electrons or positrons travel at relativistic speeds. The synchroton radiation consists of almost monochromatic high intensity x-rays within a narrow energy range, the level of which can be adjusted according to the specimen under study. [17, p. 9–11]

3.1.2 *Interaction of x-rays with matter*

The x-rays scatter and absorb in several ways when they meet matter. Consequently, the intensity of the x-rays traveling from the sample to the detector is lower than that of the incident x-rays. The drop in intensity along a straight line through the sample follows the ray-integral equation

$$\int \mu(s)\mathrm{ds} = \ln\frac{I_0}{I}, \tag{10}$$

where μ is the linear attenuation coefficient, I_0 is the incident beam intensity and I is the detected intensity. The linear attenuation coefficient is a product of density and mass attenuation coefficient. The mass attenuation coefficient μ/ρ increases strongly with increasing atomic number of the absorbent and wavelenght, or inverse of energy, of the x-rays. [17, p. 13, 21, 22] [18, p. 633]

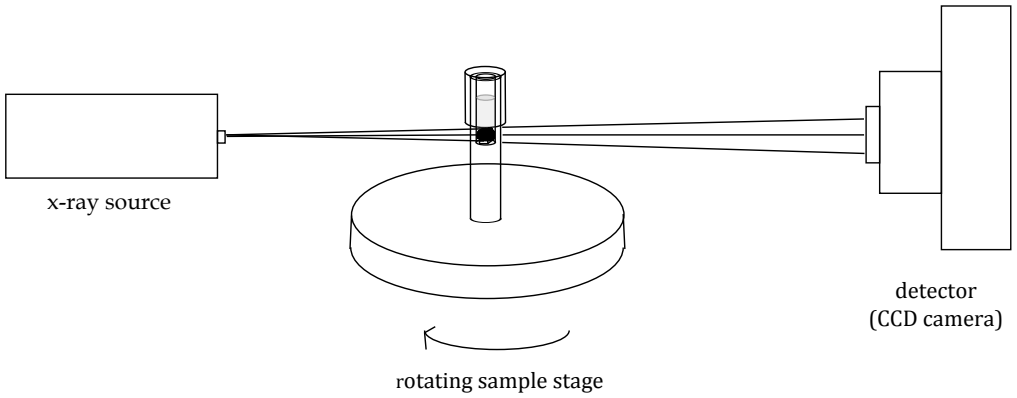

Figure 3: Principle of x-ray tomography.

3.1.3 *From projections to 3D reconstruction*

Projections show the attenuation value along a set of parallel lines. They don't, however, reveal how each voxel or volume element along that line contributes to attenuation. If a series of projections is acquired from different angles around the sample, a cross-section of the sample can be reconstructed where each pixel has the correct attenuation value. [17, p. 21, 22] [18, p. 633]

The reconstruction method used in this work is called back-projection. From each projection, lines along which attenuation takes place are added to the area of reconstruction. The attenuating mass at each pixel within the reconstrution area is obtained as a sum of attenuation values along the lines that intersect at that point. A sharpening filter is used in order to remove the additional mass generated by back-projection method. [17, p. 24–26] [18, p. 635, 636]

The filtering is carried out as follows. The Fourier transform of projections at each angle are calculated. The convolution of the projection with the filter function is computed, i.e. the Fourier transform of the projection is multiplied by the Fourier transform of the filter function. Finally, inverse Fourier transform of the convolution is taken and summed over the reconstruction plane. [17, p. 27, 28] [18, p. 636, 637]

The reconstructed data is converted to a grayscale image. Typically the resulting image is 8-bit with 256 different shades of gray. The maximum and minimum attenuation values are selected. Everything below the minimum becomes black (0)

and everything above the maximum becomes white (255). Everything between is scaled to grayscale values 1–254. As a result, in the gray scale image, the most dense parts are the brightest. [19, p. 10]

3.1.4 *Reconstruction artifacts and corrections*

The x-ray source, the tomographic device and the experimental set-up can cause several types of defects that are strengthened by reconstruction. Motion artifacts, ring artifacts, reconstruction center errors and beam hardening are some of the most usual artifacts. Motion artifacts are caused by the motion of the sample during image acquisition and appear as a blurred image. Motion artifacts can be avoided if the sample is steadily attached to the sample holder and deformation of soft structures is unabled. [17, p. 85, 86]

Reconstruction center errors arise when the center of rotation of the sample does not coincide with the reconstruction center either because its location is not precisely known or because it varies during rotation. These defects are observed as tails of apparent mass extending from the edges of the sample or pores within the sample. A useful recentering algorithm that allows the best center of reconstruction to be selected from a set of trials for a representative slice is based on the knowledge of the form of these artifacts. [17, p. 87] [18, p. 644, 646]

Ring artifacts are concentric rings that can easily distort the the separation of different phases and their geometrical shapes and thus interfere with the segmentation of the image. Ring artifacts can be reduced by smoothing of the sinograms that are plots of transmitted intensity for one row of a projection as a function of rotation angle. [17, p. 86]

When the x-ray source generates polychromatic x-rays, the softer i.e. lower-energy x-rays are absorbed in the sample more readily. This results in attenuation values that depend on the distance to the detector. The defect can be corrected for example by using a monochromatic filter or a dual energy technique. [18, p. 646–650] [17, p. 89, 90]

3.1.5 *Processing of the reconstructed images*

Reconstructed tomographic images are filtered to reduce the effect of background noise. Filtering is carried out using a variance weighted mean filter described in [20].

Many samples, especially porous ones, consist of two or more phases with distinct absorption contrast. For numerical calculations only one phase, most commonly solid, is of importance. That's why the image is segmented into solid and everything

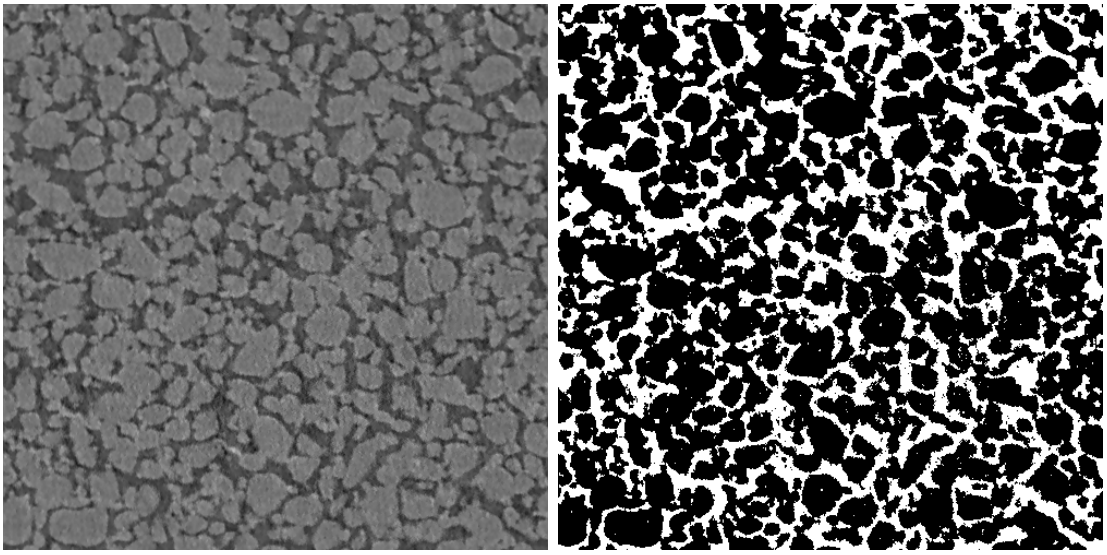

Figure 4: A reconstruction slice of sinter glass and corresponding thresholded binary image.

else. (See figure 4.) A reasonable threshold value, which separates the solid material from other phases, is selected. Everything above that value is then turned to white and everything below it to black. The resulting image has only two phases: solid (black) and void (white). [17, p. 119, 120]

3.1.6 *Equipment*

In this study samples of the four sample materials were prepared for x-ray tomography. The same physical sample was scanned first dry and then in saturated state in water environment in order to get comparable data for flow simulations. For this purpose two different x-ray micro-CT devices were used, the ScyScan 1172 desktop device for imaging the press felt sample and the more advanced XRadia MicroCT-400 for other materials.

SkyScan 1172 is a compact desktop apparatus for x-ray micro-CT (see figures 5 and 6). It has an x-ray tube with a spot size of 5 µm operating at 20–100 kV and 0–250 µA. The rotating sample holder can be moved vertically in order to adjust the optimal sample position. The detector is a 10 megapixel (4000x2300) CCD camera. With maximum magnification a nominal resolution close to 1 µm can be achieved. [19]

Xradia MicroCT-400 is an effective apparatus for research. A selection of objectives for different purposes and a wide variability of geometrical magnification is provided with the 4 megapixel CCD camera. A resolution of around 1 µm and a

pixel size of 0.56 µm is achievable. The objective lenses are specifically designed to enhance the contrast of even the lightest materials.

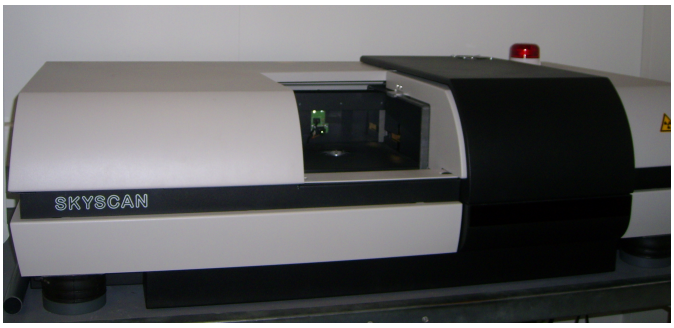

Figure 5: An overview on SkyScan 1172 with the sample stage door open.

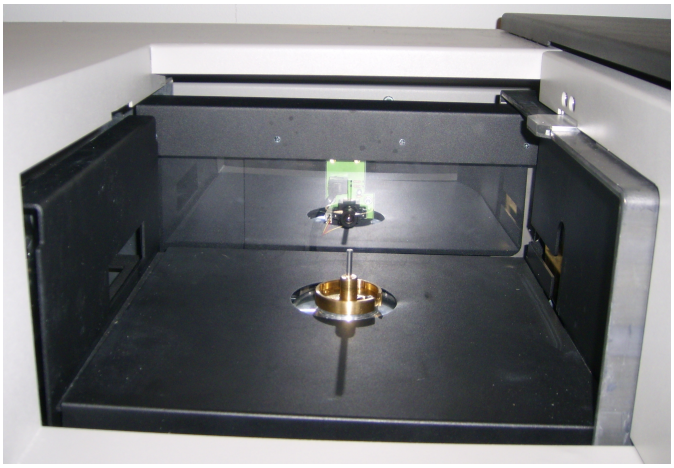

Figure 6: A close-up of the sample stage: the x-ray source on the right, the sample holder in the middle, the detector on the left, and a visual camera (for optimizing sample position) in the back.

3.2 Numerical analysis of tomographic images

3.2.1 *Pore size analysis*

Pore sizes in a porous material can be determined numerically e.g. by fitting spheres into the pore space [6, p. 41]. The sphere is centered at a voxel in the pore volume. The pore size at that particular point is defined as the maximum radius of the sphere fully included in the pore space. Pore size distributions for the sample materials in this work were calculated using a program based on this principle. The outcome was given in pixels and proportions and the data was converted into micrometres according to the pixel sizes of the images.

3.2.2 *The Lattice Boltzmann method*

The Boltzmann equation describes reversible Newtonian single particle dynamics applied to a fluid under the so called Stosszahlansatz approximation, i.e. to dilute fluid with short-lived and short-range intermolecular interactions. The Navier-Stokes equations, expressions of mass and momentum conservation in fluid dynamics, can be derived from the Boltzmann equation using the Chapman-Enskog procedure, a multiscale method which enhances the stability of numerical calculations. [5, p. 6, 7, 11–13].

The Lattice Gas Cellular Automata method is based on the fact that a hexagonal lattice with identical lattice particles, only one allowed speed and six allowed propagation directions can reproduce the equations governing real fluid flow. Subtituting Boolean occupation number in the LGCA model with one particle distribution function one arrives at the general Lattice Boltzmann Equation or non-linear LBE. The benefit of LBE compared to LGCA is the disappearance of statistical noise. [5, p. 17–42]

In this work LBE is applied to flow in a porous medium. The binary matrix of solid and void served as the basis for the knowledge where the flow is possible. The actual fluid flow was solved with no-slip boundary condition, i.e. zero flow velocity on the solid boundaries. [5, p. 82–84, 110–122]

3.3 Permeability measurements

Permeability of a material is traditionally determined by measuring the pressure gradient across a sample and the flow velocity through the sample. In this work a permeability device based on this principle was used to study the flow through the porous sample materials (see figures 7, 8 and 9). The main part of the device is composed of two cylinders between which the sample is placed. Pressurized air or water is driven into the lower chamber and proceedingly through the sample into the upper chamber. The required data for the pressure difference is acquired with a differential pressure sensor between the lower and the upper chamber and a pressure transducer connected to the upper chamber i.e. downstream. Water flow is measured with a magnetic volumetric flow meter and air flow rate with a thermal mass flow meter.

To determine permeability of press felt, synthetic chammy and cardboard five circular samples of about 10 cm in diameter were used. The samples were placed freely between the upper and lower chambers their edges compressed tightly between the edges of the chambers to prevent flow past the sample. The diameter of the effective flow area was approximately 7.8 cm. The sinter glass sample was glued in a plastic sample holder with a conduction hole of 2.3 cm in diameter.

The measurements with air were carried out using a LabView program which automatically raises the control voltage of pressure at the upstream by the selected amount, lets the flow stabilize and takes measurements up to the limit where the volumetric flow reaches the maximum of the flow meter. The measurements with water were carried out with a similar program where the raise in the control voltage and the capturing of measurements were performed manually.

The experimental data was analysed statistically. A least mean square linear fit was done for each sample material singly for each of the ten measurements with air and five measurements with water. Sinter glass was an exception with only four measurements with air and two with water. The procedure gave an estimate of permeability and its error for each measurement. The permeability of each sample material was determined as the mean of these individual permeability values. The maximum error of the mean value was estimated by quadratic combination of the standard error and the mean of the errors of invidual LMS fits.

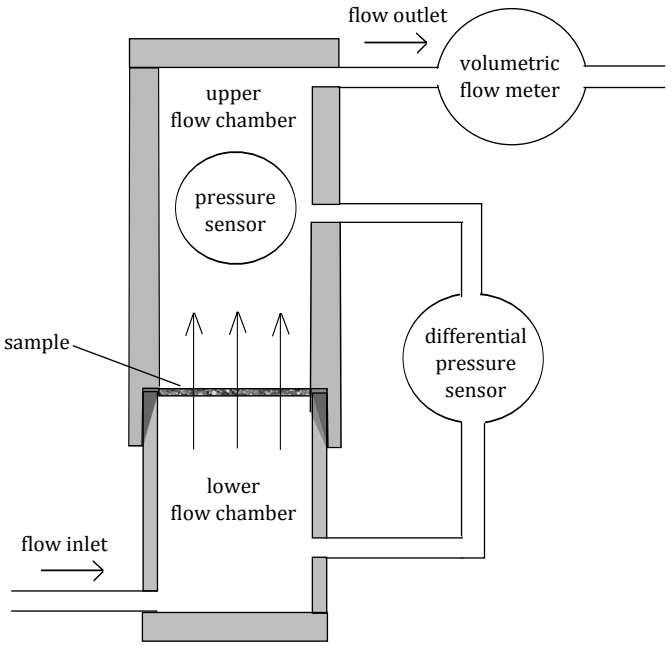

Figure 7: The principle of permeability measurement.

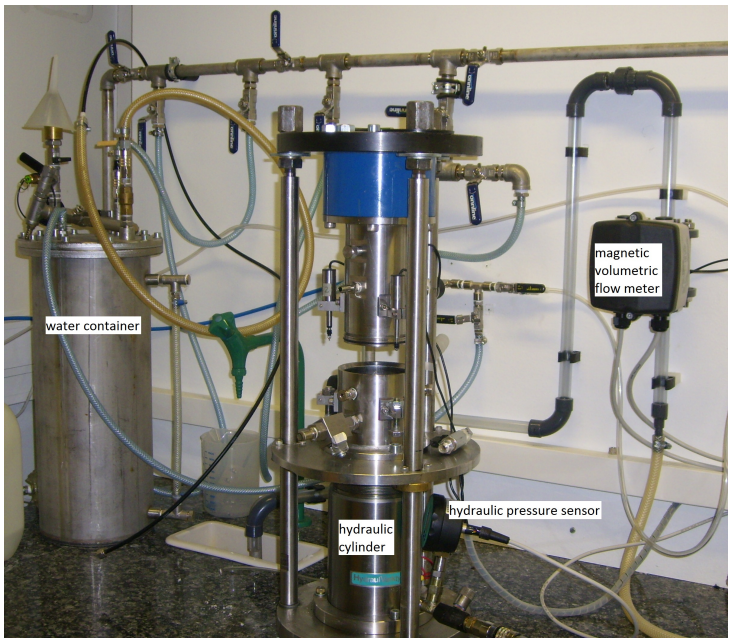

Figure 8: Permeability device, water container, hydraulic cylinder and sensors.

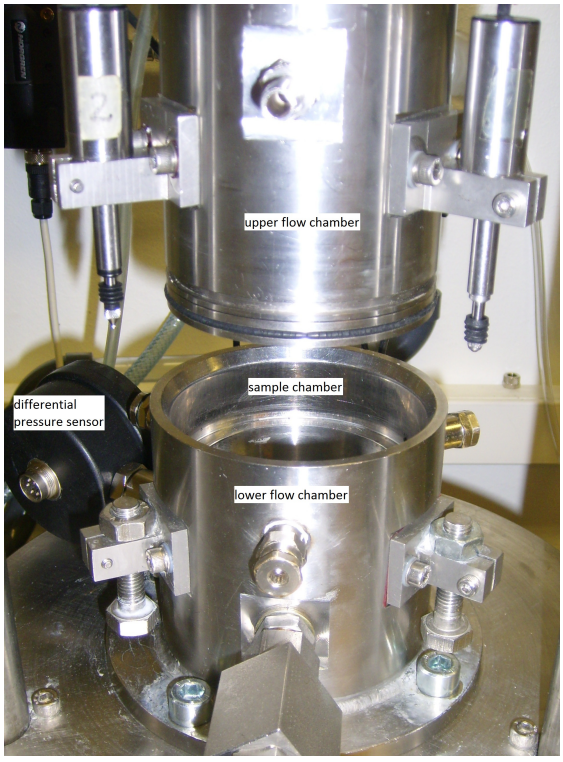

Figure 9: A close-up of flow chambers and differential pressure sensor.

4 Results

4.1 Tomographic imaging

4.1.1 *Sample materials*

Sample materials were chosen so that they differ in constitution, structure, permeability and response to introduction of water. Originally there were seven different porous materials under examination. The four materials for this study were selected according to their suitability for obtaining accurate tomographic images and running reliable permeability measurements. The sample materials used are press felt, synthetic chammy, sinter glass and cardboard.

4.1.2 *Sample holders and sample preparation*

A special sample holder designed to contain water was prepared for this study (see figure 10). It has the shape of a cylinder about six millimetres in diameter and from the top to the halfway there is an aperture of two millimetres in diameter. On the top of the sample holder a cap is used to prevent water from evaporating while x-ray tomography is in progress.

One of the biggest weaknesses of the sample holder is the necessity to bring the water in contact with the sample from above. This is definitely not the most controlled way to wet the sample because of its risk of remaining air pockets inside the sample as well as between the sample and the sample holder wall. An idea of a sample holder with a more complex structure that enables watering through capillary action and slow penetration was developed but not yet realized within this study.

Most of the softer samples were squeezed from a sheet of sample material with a hollow circular blade. The cardboard sample was a circle of about 1.5 millimetres in diameter. The fibres of press felt were too sizeable for such small a sample, which is why it was scanned with SkyScan in a hand-tailored sample holder similar to the original one. The press felt sample was also circular and about 6 millimetres in diameter. Lots of samples of synthetic chammy were wasted because of the efforts to remove air from the sample damaged its structure. The scanned sample was cut from a sheet using a paper knife and was rectangular, about 1 mm $\times$ 1 mm. The sample of sinter glass was sawn from a glass sinter. The sample had more or less the shape of rectangular cylinder with a cross-section of about 2 mm $\times$ 2 mm.

Before scanning, the sample had to be properly attached to the sample holder so that it would remain virtually untouched during and between the scans. The sample was attached to the bottom of the aperture in the sample holder with two-sided tape.

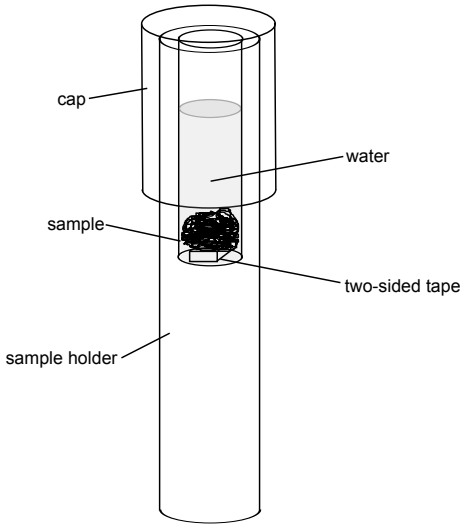

Figure 10: Sample holder.

4.1.3 *Wetting of the samples*

The wetting of the samples was done with ion-exchanged water. A syringe was used for the purpose. However, air pockets and bubbles remaining inside and around the sample created a severe problem that was not readily solved. The density of air and water are crucially different and accidental air makes the distinction of the sample features in water environment even more challenging. The air-water interfaces may cause distortions that wipe out prominent data of the structure of the sample.

Most of the air bubbles could be removed just by tapping the sample holder with fingers. Some of the air attached to walls of the sample holder were removed using the injection needle. In the case of synthetic chammy nothing seemed to work. A dilute solution of soap was enough to prevent air pockets from remaining inside the sample.

4.1.4 *Experimental set-up*

The press felt sample was scanned with SkyScan and the other materials with XRadia. Before the scan can be started, there are some parameters to be set. These include source voltage and current and exposure time. All of these affect the contrast of the image.

The dry press felt sample was scanned with default values of source voltage and current. The appropriate exposure time was selected taking radiographs with dif-

Table 1: Imaging settings for x-ray tomography.

sample		source voltage [kV]	source current [μA]	optical magnification	exposure time [s]
press felt	dry	100	100	-	2.356
	wet	100	94	-	5.301
chammy	dry	20	200	9.825	90
	wet	20	200	3.96	500
cardboard	dry	40	50	9.825	45
	wet	40	50	9.825	120
sinter glass	dry	20	200	3.96	60

sample		source to sample distance [mm]	detector to sample distance [mm]	pixel size [μm]
press felt	dry	78.2	217.9	4.08
	wet	78.2	217.9	4.08
chammy	dry	60	6	1.2492
	wet	60	150	0.974
cardboard	dry	60	57	0.7046
	wet	60	57	0.7046
sinter glass	dry	60	50	1.8595

ferent exposure times. The rotation angle between each shot was given the value 0,5°. One reference frame per ten radiographs was set to be taken in order to diminish noise caused by background radiation. The wet sample was scanned in potassium iodide solution and the source current was reduced a little to enhance contrast. The required exposure time in order to gain suffient contrast was more than twice the time that the dry sample took. Otherwise the same imaging settings were used as with the dry sample. (See table 1.)

With Xradia some more adjustment can be done before scanning. The sample stage can be moved in all three directions to make sure of straight alignment. This is done by taking a radiograph from three different angles 90 degrees apart and choosing the wanted center of reconstruction. Different objectives are also available, which makes it possible to scan a certain sample from more than one distance with the same resolution.

The cardboard sample was scanned in the so-called absorption mode, where the source is at fixed distance from the sample and the detector is brought as near as possible to the sample. Rotation angle and reference frames were set similarly to

SkyScan. The dry and wet sample were scanned with identical settings excluding exposure time, which was nearly three times longer for the wet sample.

The sample of synthetic chammy was scanned dry similarly to cardboard. The scanning of the wet sample, however, was done in the so called phase contrast mode, where the source stays still but detector is moved away from the sample. This decision was made in order to experiment if the phase contrast mode would live up to its name and help to distinguish water from the solid material. The price to pay from this trial was the prolonged exposure time and image resolution different from that of the dry sample.

Sinter glass was only scanned dry because its structure was not expected to undergo any changes due to water. This reasoning actually should have led to an opposite decision considering the reference it would have served to the three other materials that in turn were expected to swell in water.

4.2 Image processing and approximate remarks

After reconstruction, correction of artifacts and filtering the tomographic images were prepared for numerical study. In order to grasp the research problem, the same physical domain of the sample has to serve as the basis for numerical analyses whether the sample was scanned dry or wet. The determination of these domains from each tomographic reconstruction was a time-consuming process that was carried out approximately and manually.

The tomographic reconstructions of dry and wet sample were viewed side by side. The goal was to crop domains of both images that are not of same size but that enclose the same part of the fibrous network as precisely as possible. The images of dry and wet sample were rotated to achieve the same orientation. Common features were then sought from the dry and wet material. The same fibres, or the same parts of them, were then cropped in as large a domain as possible within the reconstruction area. Cropping was carried out step by step browsing the reconstruction slices back and forth until the selected area seemed functional throughout the sample. No preconditions of the size of the cropped area were set besides that in plane the materials were assumed to swell in equal amounts in all directions.

The cropped tomographic grayscale images (see figures 11, 12 and 13) provide information about the effects of wetting on the structure of the material and the amount of noise and artifacts as well as the contrast between the solid and fluid phases in the tomographic reconstruction of the sample. Concluded from the cropped images, the three fibrous sample materials swell in a similar amount in plane, approximately 4 to 5 %.

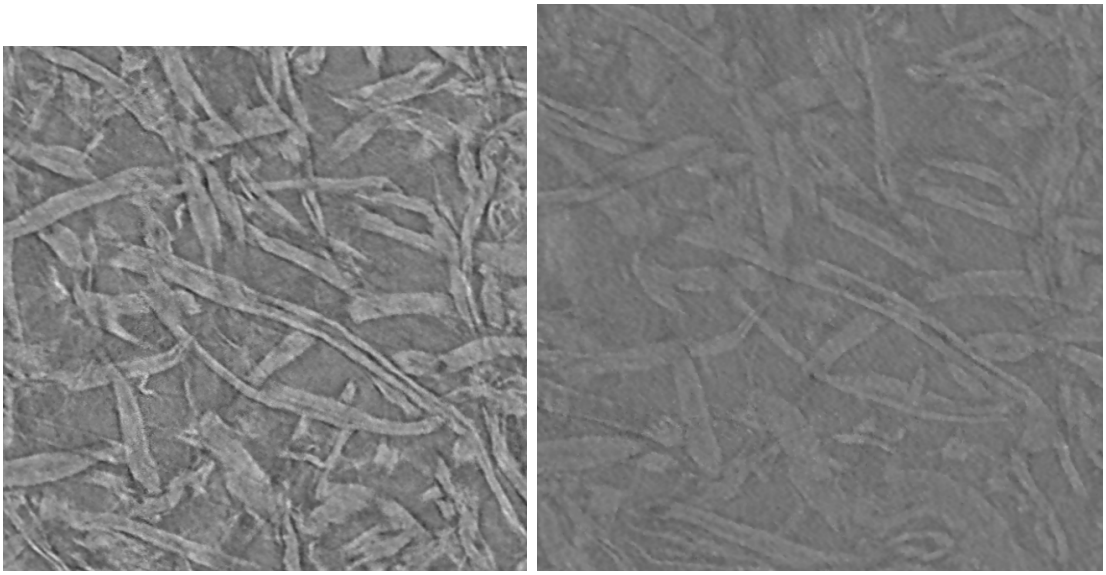

Figure 11: Tomographic grayscale images of dry (on the left) and wet cardboard.

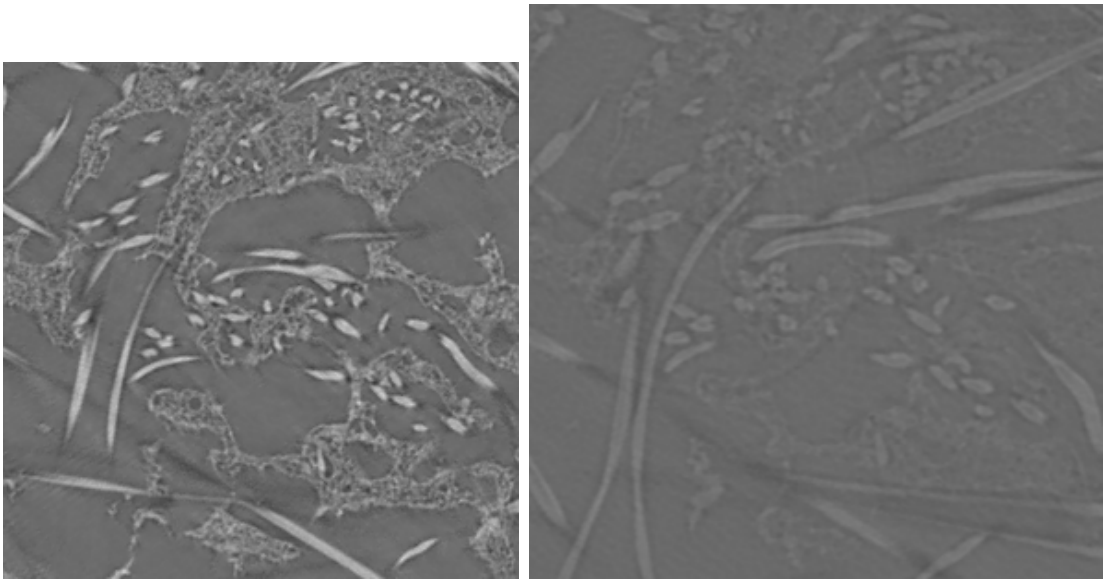

Figure 12: Tomographic grayscale images of dry (on the left) and wet synthetic chammy.

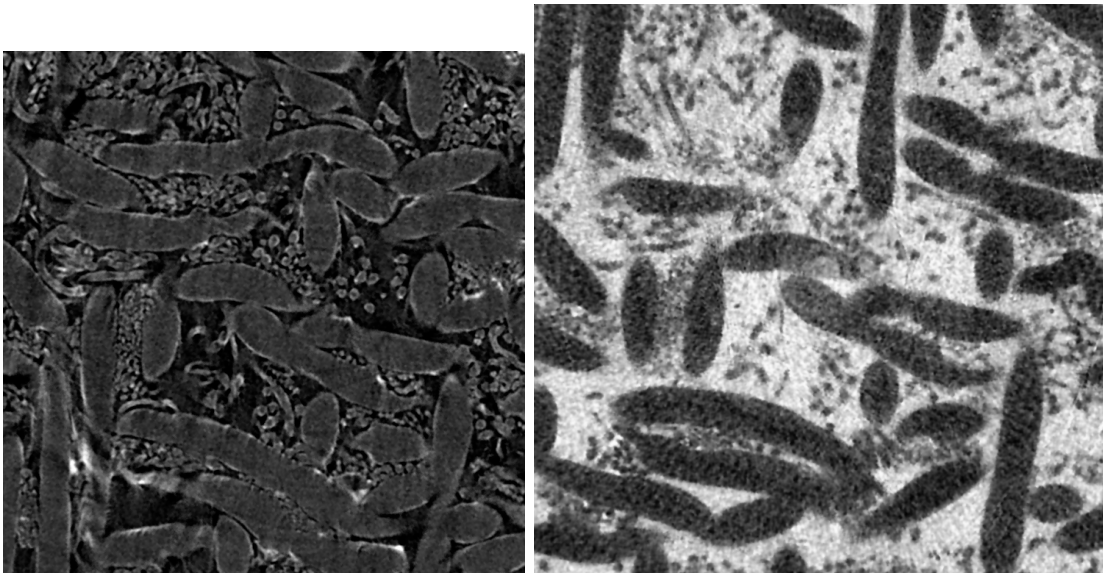

Figure 13: Tomographic grayscale images of dry (on the left) and wet press felt.

There is more variation in the amount of swelling in thickness direction. The thickness of press felt increased by 7 %, whereas with chammy the amount of swelling was 12 % and with cardboard as much as 29 %. The influence of this type of swelling is seen in the tomographic images as displacement of certain fibres. A reconstruction slice at the corresponding height of dry and wet sample does not include similar cross-sections of all the fibres that cut through it. This makes the approximate cropping of the images challenging.

In the case of all three water-absorbing sample materials scanning in water environment causes a prominent deterioration of image quality. The phase contrast of the images acquired of samples in water environment was worse with all three materials. In the case of cardboard (see figure 11) even the dry sample generated a smeary image. The thresholding of the images was a struggle between trying to keep the fibre walls intact and excluding the non-fibrous material emerging from noise.

The tomographic imaging of synthetic chammy was the most successful of all the sample materials. This also goes for the wet sample. From the tomographic reconstruction of wet chammy, the fibres are clearly distinguishable but smaller details in the structure are not as visible. There are also some ring artifacts remaining in the reconstruction. (See figure 12.) However, despite the poorer contrast, there is not much noise in the image that would decrease the numerical permeability considerably. Even the lumens that open up within the fibres due to water absorption are readily detected.

The tomographic imaging of press felt with SkyScan was sufficiently accurate with regard to the dry sample but apparently poor with the wet sample. There are some openings inside the larger fibres in the tomographic image of dry press felt. These are absent in the image of the wet sample which again is crowded with noise that distorts telling apart the smaller fibres and generates additional voxels that appear as solid, which affects the numerical permeability in an undesirable manner.

4.3 Numerical analysis

The goal of this work is to find a way to take such accurate tomographic images of wet samples that they would enable reliable numerical analysis. One of the ways to examine the outcome is to compare it to the data from the tomographic images of the same physical sample but dry.

4.3.1 *Pore and fibre size distributions*

Pore size distribution was calculated for every sample material both dry and wet. The tomographic images of cardboard, even dry, were so scruffy that they did not give any reliable data. The glass sinter was scanned only dry, which seems to make a great difference because pore size distribution analysis would have shown if the tomographic images of dry and wet sinter glass would have generated statistically identical pore structure, as they ideally would.

For press felt and synthetic chammy the pore size analysis gave fairly reasonable results. The fibre size analysis was also run with the same method when black and white were interchanged in the images. The outcome for press felt indicates a drop of 25 % in average pore size of press felt and a 5 % increase in average fibre radius. These changes result in a 29 % higher porosity than before wetting. (See table 2.)

As for synthetic chammy, the mean pore size of wet sample is 28 % smaller than that of the dry sample. The fibre radius instead increased by 56 %. The resulting porosity is 2 % lower than before watering.

The fibre size distribution of press felt is a good estimate for the compatibility of the numerical analysis of dry and wet samples because press felt is composed of two distinct fibre sizes (see figure 14). The result is evident in figure 15. The form of the distribution is similar with dry and wet press felt but the shift of the maxima due to swelling of fibres is also clearly seen.

The pore size distribution of synthetic chammy (reconstruction slices in figure 16) was illustrated as a graph from which dry and wet sample are hardly separated (see figure 17). This indicates that this kind of numerical analysis is as reliable for the tomographic image of wet chammy as for dry.

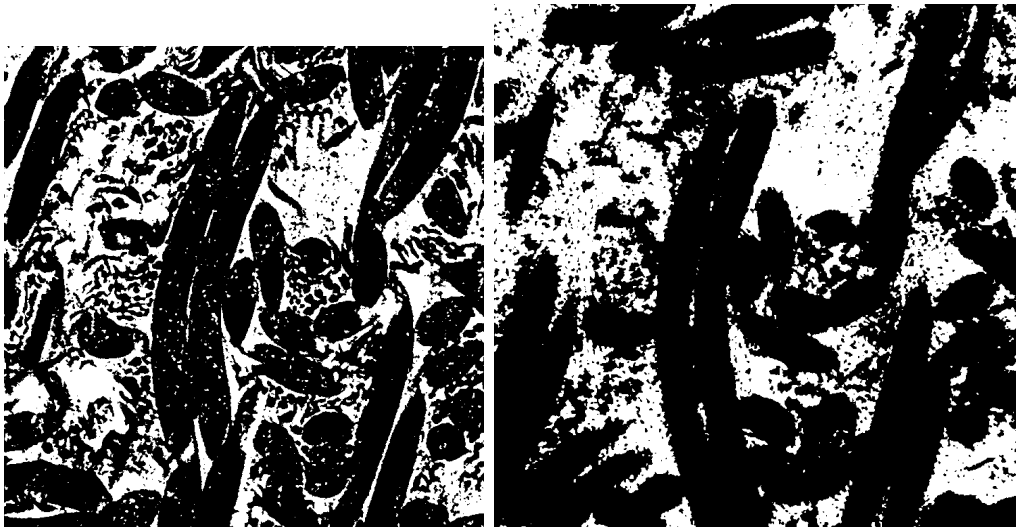

Figure 14: Tomographic images of dry (on the left) and wet press felt after segmentation.

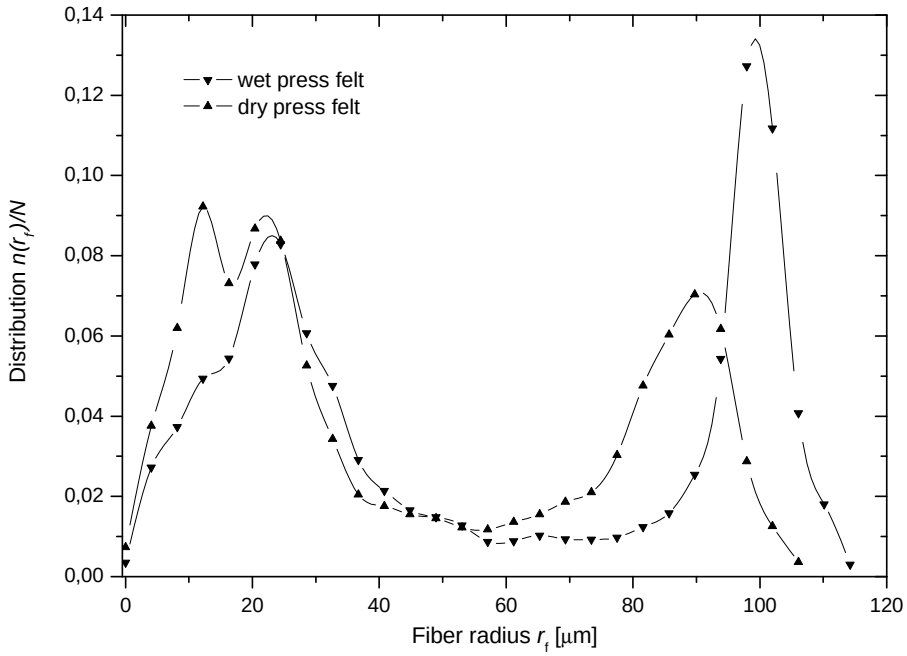

Figure 15: Fibre size distribution for dry and wet press felt.

Figure 16: Tomographic images of dry (on the left) and wet synthetic chammy after segmentation.

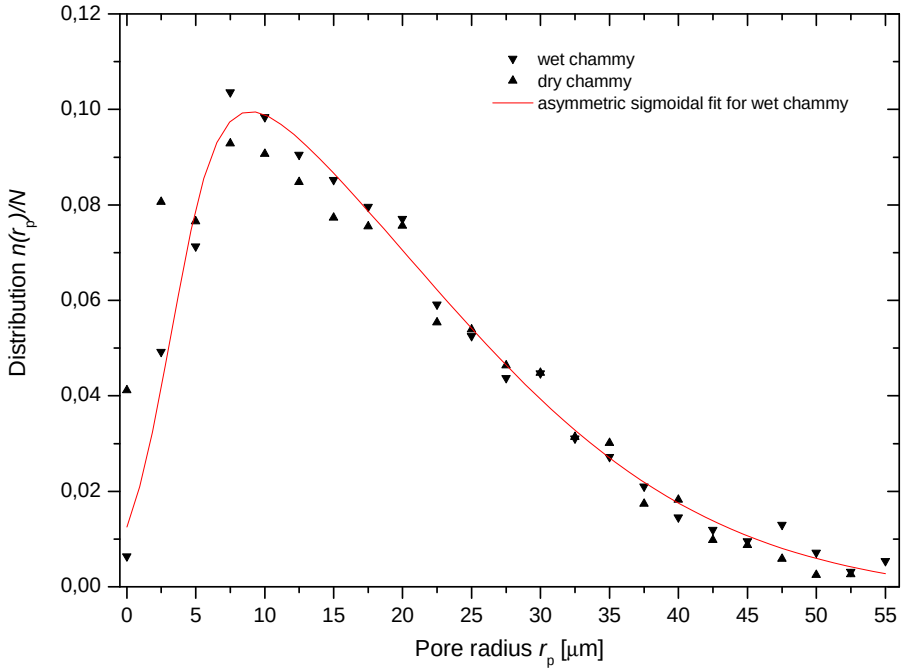

Figure 17: Pore size distribution for dry and wet chammy.

Table 2: Results from pore size distribution analysis and Knudsen numbers.

Material		Porosity ϕ	Mean pore radius r_p [µm]	Mean fibre radius r_f [µm]	Knudsen number of air flow Kn
Press felt	dry	0.317	37.1	16.8	0.00092
	wet	0.409	27.8	17.7	–
Synthetic chammy	dry	0.816	12.5	2.09	0.0027
	wet	0.798	8.98	3.26	–
Cardboard	dry	0.564	2.22	–	0.015
	wet	0.565	1.91	–	–
Sinter glass	dry	0.318	4.47	–	0.0076

4.3.2 *Permeability for air and water*

Despite the differences in constitution, numerical values of permeability of press felt, synthetic chammy and sinter glass are of the same order of magnitude, 10^{-12} m^2. The numerical permeability of cardboard is smaller by one order of magnitude, 10^{-13} m^2. (See table 3.) All three sample materials that were expected to swell in water also have lower permeability for water than for air. Structural changes due to wetting seem to be the most likely explanation for the difference apparent in experiments long before.

Synthetic chammy which according to pore size analysis also undergoes quite a drastic raise in fibre thickness and a subsequent drop in pore size has the most distinct deviation in permeability values. The permeability of chammy for air is more than twice the permeability for water. The magnitude of the change may be a surprise but the quality of the tomographic images in the case of chammy is so good that the noise is not to blame for the outcome.

Press felt also has a remarkable difference in the two permeability values. The numerical analysis for the dry sample results in a value 57 % larger than that for the wet sample. In the tomographic image of the wet press felt sample some structural details especially of the thinner fibres are missing, which may explain the anomalies in the pore size analysis. Interestingly, this seems to have no effect on the numerical permeability values that differ in the predicted manner.

With respect to numerical analysis, cardboard permeates air more efficiently than water as well. The difference, however, is only 7 %, which is surprising. It would seem probable that a pulp product would swell by an amount large enough to

Table 3: Numerical and experimental values of permeability.

Material		Air permeability K_a [10^{-12} m^2]	Water permeability K_w [10^{-12} m^2]	Ratio K_a/K_w
Press felt	num.	7.4	4.7	1.57
	exp.	9.4 ± 0.3	7.2 ± 0.7	1.31 ± 0.13
Synthetic chammy	num.	3.4	1.56	2.2
	exp.	5.4 ± 0.2	1.62 ± 0.10	3.4 ± 0.3
Cardboard	num.	0.238	0.22	1.07
	exp.	0.269 ± 0.004	0.28 ± 0.03	0.96 ± 0.08
Sinter glass	num.	3.10	–	?
	exp.	2.71 ± 0.02	3.0 ± 0.4	0.90 ± 0.10

lower the permeability much more. The bad quality and noisiness of the images might be the reason behind this unexpected behaviour. (See table 3.)

The sample materials used in this work have values of permeability of order 10^{-13} to 10^{-12} m^2. According to findings from the earlier experiments, the Klinkenberg effect is significant when permeability is below 10^{-18} m^2 [14]. In this light the Klinkenberg effect would not have any influence on the air permeability of the sample materials.

However, the Knudsen numbers of chammy, sinter glass and cardboard calculated from equation 7 for air flow at ambient pressure [21] are of same or higher order of magnitude than 0.001 (see table 2), which means that they are in slip flow region [13]. Although the Klinkenberg effect may be unimportant for air flow through press felt, chammy and sinter glass, in terms of Knudsen number it should slightly affect the air flow through cardboard.

4.3.3 *Comparison with experimental values of permeability*

The difference between air and water permeability was originally discovered with experiments. Therefore the comparison of the numerical values of permeability to experimentally determined values is one of the most important ways to estimate the capability of x-ray tomography to study the subject. In addition, or perhaps above the actual permeability values, the ratio of values of permeability for air and water is of interest.

All the experimental results are of the same order of magnitude than the numerical ones. In this case, results do give reason to believe that the structural changes

apparent in tomographic images are in fact the reason why deformable porous materials permeate water less than air.

As for press felt, the evident separation of values of permeability for dry and wet sample solved numerically is also clearly seen in measurements with air and water. The experimental values of permeability are higher than the numerical ones, by 27 % for air and by 53 % for water. However, the ratio of air and water permeability solved numerically exceeds the experimental value only by 20 %.

In the case of synthetic chammy, the experimental permeability for air is 58 % larger than the numerical value. The values of permeability for water instead differs by only 4 % and the numerical result actually falls within the error bars of the experimental one. The ratio of experimental values of permeability for air and water is 55 % larger than the numerical value but it is still of the same order of magnitude and easily separated from the ratios for other sample materials that are significantly smaller.

The experimental values of permeability of cardboard are also higher than the numerical ones. The values of permeability for air differs by 13 % and for water by 27 %. In this case, the ratio of the experimental values of permeability is 11 % smaller than that of the numerical values. The permeability for water determined experimentally was surprisingly higher than for air. This may, however, be explained by experimental uncertainty.

5 Conclusions

Several studies on difference of permeability for air and water have been carried out. The studies that are dealt with in section 2 of this thesis cover a range of non-swelling natural or synthetic materials. The causes for the differences may however be quite diverse when swelling materials with higher values of permeability are considered. The Klinkenberg effect has little effect on the air permeability of the materials in this work.

Defining permeability of porous materials using x-ray tomography is a novelty that has been used for only a short time. The goal of this work is to find a way to image the same sample of a porous material dry and wet in order to simulate flow through both structures. The numerical values of permeability of dry and wet sample reveal if the change in pore structure explains the previous experimental discovery. The permeability experiments carried out with same sample materials confirm the numerical outcome.

The most important conclusion from the experimental part of this work is that the goal was achieved. The pore size analysis of tomographic reconstructions of press felt and synthetic chammy give rational results also when the sample was wet. When the images are thresholded for flow simulation, the main part of the structure of the porous network is retained. In all cases the numerical values of permeability of dry and wet material is of the same order of magnitude, but as expected, the permeability of wet material is lower. The same behaviour is observed experimentally. The amount in which the permeability for air and water differ is distinct for each material. The numerical and experimental values for ratio of values of air and water permeability are much closer to one another than the ratios of different materials.

Almost all numerical permeability values are slightly lower than the corresponding experimental ones. Moreover, the ratio of the numerical values of permeability for air and water is larger than that of the experimental values for press felt and cardboard. This may at least for some part be explained by noise in the images that is especially a problem with wet samples. More effort should be made to reduce the noise in the images so that no additional solid voxels besides the actual sample material would remain in the binary images.

Altogether the outcome of the Lattice Boltzmann method in determining the permeability of wet porous materials was surprisingly successful. X-ray tomography and numerical analysis are useful tools for studying porous materials also in water-saturated state. The method still needs to be improved in order to provide more reliable data.

A good reference for the swelling fibrous materials used in this work would be a

granular non-swelling medium like sinter glass. The biggest mistake that makes its inclusion in the research nearly vain is the fact that it was imaged with x-ray tomography only with a dry sample. The numerical value of its water permeability would have a great value when the effects of swelling and noise to the permeability values are evaluated. However, according to the findings within this work, it is safe to state that the constructional changes caused by water penetration are a major factor in the decrease in permeability when pore fluid is exchanged from air to water.

Tomographic imaging of water-saturated samples is still an issue to work out. The development of a sample holder where the sample could be wetted from below would be the next step towards a more successful scan of a wet sample. When the sample is watered and the air absent, the contrast of the image is the next challenge. Much exploration on the effect of the imaging settings on phase separation is ahead for anyone that feels up to the challenge. For optimal image quality, the true impact of the voltage and current of x-ray source, the exposure time and the distance from the sample to the detector should be recognized and taken into account.

Other subjects for further research might be closer examination of the structural changes caused by wetting in different materials and their influence on the permeability of these materials. The effect of the deformation of single fibres on the pore structure and thereby on permeability could be studied with nano-CT. This detailed knowledge of the consequences of water intrusion could help to complete the overall picture of the problem of difference in air and water permeability of porous media.

References

[1] G. Carlsson, T. Lindström and B. Norman: *Some basic aspects on wet pressing of paper*, International Water Removal Symposium, Vancoucer, 1982.

[2] F. A. L. Dullien: *Porous Media – Fluid Transport and Pore Structure*, p. 157, 170–172 Academic Press, Inc. 1979.

[3] Viivi Koivu, Keijo Mattila, Markku Kataja: *A method for measuring Darcian flow permeability of thin compressed fibre mats*, Nordic Pulp and Paper Research Journal Vol 24 no. 4/2009.

[4] Viivi Koivu: *Analysis of fluid flow through porous media based on x-ray micro-tomographic reconstructions*, University of Jyväskylä, 2010.

[5] *The Lattice Boltzmann equation for Fluid Dynamics and Beyond*, Sauro Succi, Clarendon Press, Oxford, 2001.

[6] Jacob Bear: *Dynamics of Fluids in Porous Media*, p. 14, 41, 43, 44, 50, 51, 111, 120, 121, 128, American Elsevier Publishing Company, Inc. 1972.

[7] Kaarlo Niskanen: *Papermaking science and technology Part 16: Paper Physics*, p. 288, Helsinki Fapet, 1998.

[8] L. J. Klinkenberg: *The Permeability of Porous Media to Liquids and Gases*. Production Practice, p. 200–213, American Petroleum Institute, 1941.

[9] Leo Neimo: *Papermaking science and technology Part 4: Papermaking Chemistry*, p. 152–158, Fapet, Helsinki, 1999.

[10] T. Forseth, T. Helle: *Effect of moistening on cross sectional details of calendered mechanical paper.* Presented in 82nd annual meeting of CPPA, 1996.

[11] Alfred J. Stamm, Harold Tarkow: *Penetration of cellulose fibers.* Forest Products Laboratory, Forest Servicem U.S. Department of Agriculture. Recieved April 27, 1949.

[12] J. Chastanet, P. Royer, J.-L. Auriault: *Does Klinkenberg's Law Survive Upscaling?* Transport in Porous Media 56, p. 171–198. Kluver Academic Publishers 2004.

[13] Maria Cecilia Bravo: *Effect of transition from slip to free molecular flow on gas transport in porous media*, Journal of Applied Physics 102, 074905, American Institute of Physics, 2007.

[14] W. Tanikawa, T. Shimamoto: *Klinkenberg Effect for Gas Permeability and Its Comparison to Water Permeability for Porous Sedimentary Rocks.* Hydrology and Earth System Sciences Discussions 3, p. 1315–1338, 2006.

[15] Yu-Shu Wu, Karsten Pruess, Peter Pershoff: *Gas Flow in Porous Media with Klinkenberg Effects*, Transport in Porous Media 32, p. 117–137, Kluver Academic Publishers, 1998.

[16] D. R. Faulkner, E. H. Rutter: *Comparisons of water and argon permeability in natural clay-bearing fault gouge under high pressure at 20 °C.* Journal of Geophysical Research, vol. 105, no. B7, p. 16, 415–426, July 10, 2000.

[17] Stuart R. Stock: *MicroComputed Tomography: Methodology and Applications.* Taylor & Francis Group, LCC. CRC Press, 2009.

[18] John C. Russ: *The Image Processing Handbook*, 5th Edition, p. 629–666. Taylor & Francis Group, LCC. CRC Press, 2007.

[19] *SkyScan1172 Desktop X-ray Microtomograph Instruction Manual*, SkyScan, Belgium, 2005.

[20] Rafael C. Gonzalez, Richard E. Woods: *Digital Image Processing*, 2nd Edition, p. 239–241. Prentice-Hall Inc. 2002.

[21] S. Jennings: *The mean free path in air.* Journal of Aerosol Science 19 (2), 1988, p. 159.

Attachments

Figures from permeability measurements

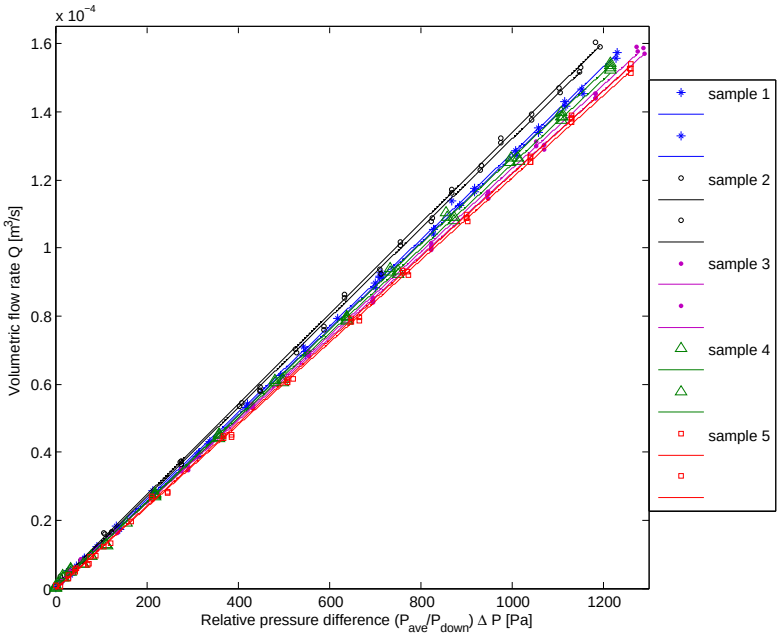

Figure 18: The relative pressure difference across the cardboard sample as a function of air volume flow.

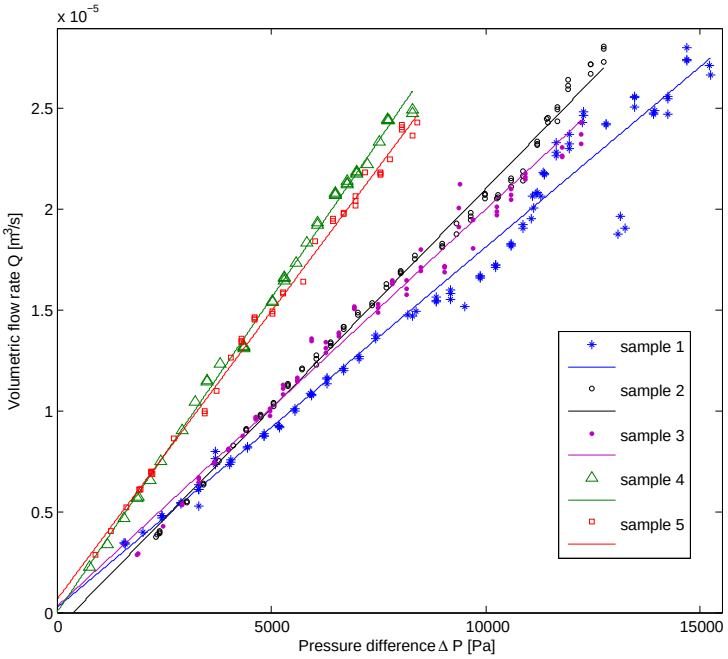

Figure 19: The pressure difference across the cardboard sample as a function of water volume flow.

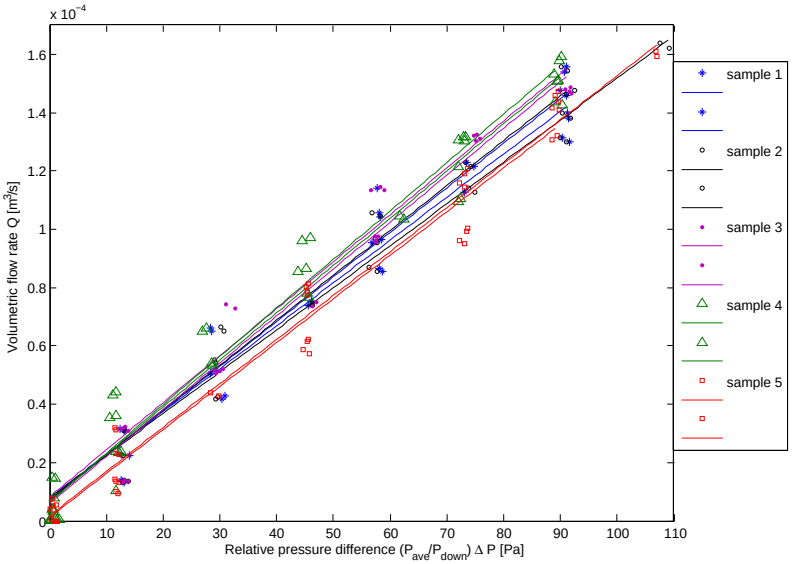

Figure 20: The relative pressure difference across the chammy sample as a function of air volume flow.

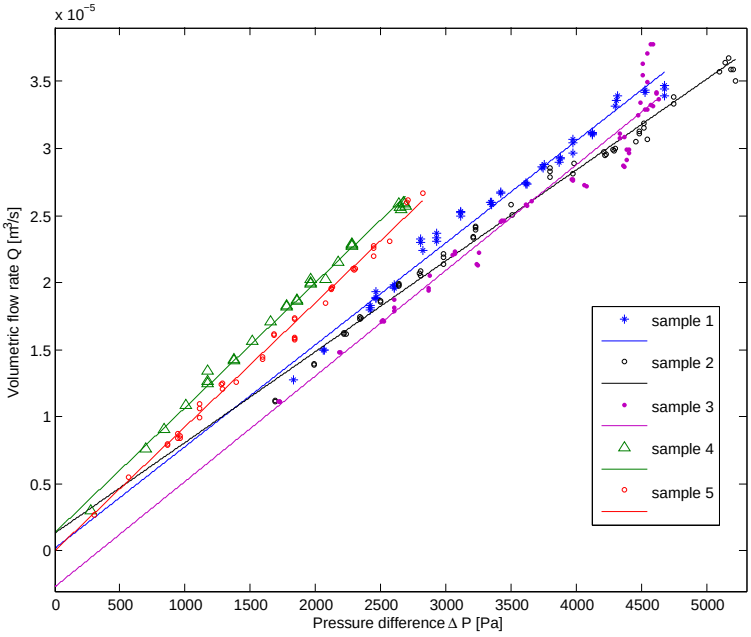

Figure 21: The pressure difference across the chammy sample as a function of water volume flow.

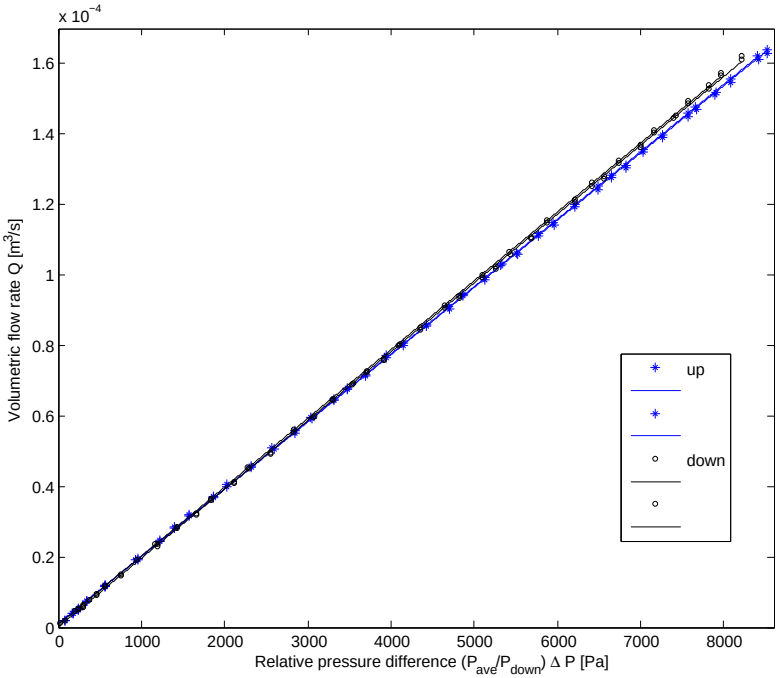

Figure 22: The relative pressure difference across the sinter glass sample as a function of air volume flow.

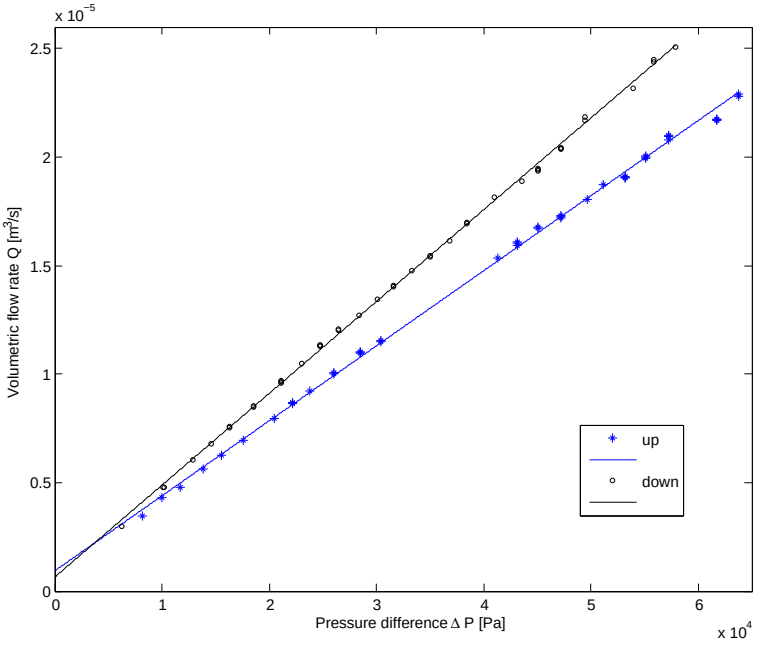

Figure 23: The pressure difference across the sinter glass sample as a function of water volume flow.

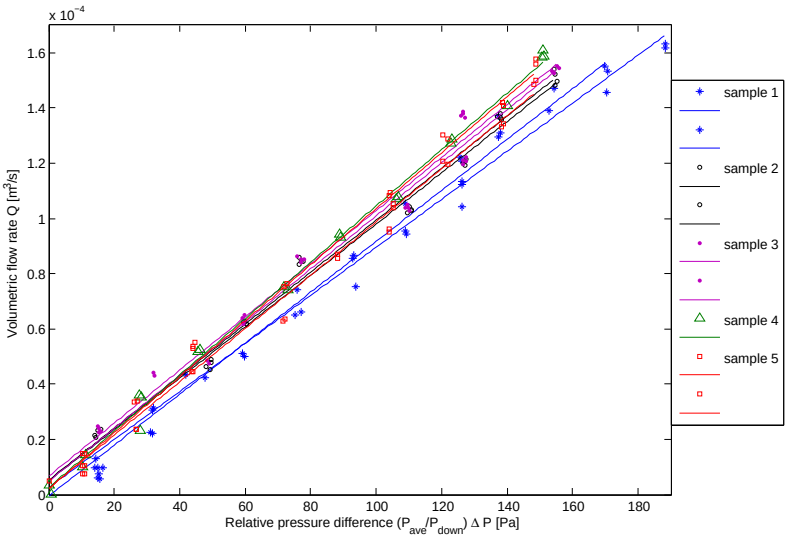

Figure 24: The relative pressure difference across the press felt sample as a function of air volume flow.

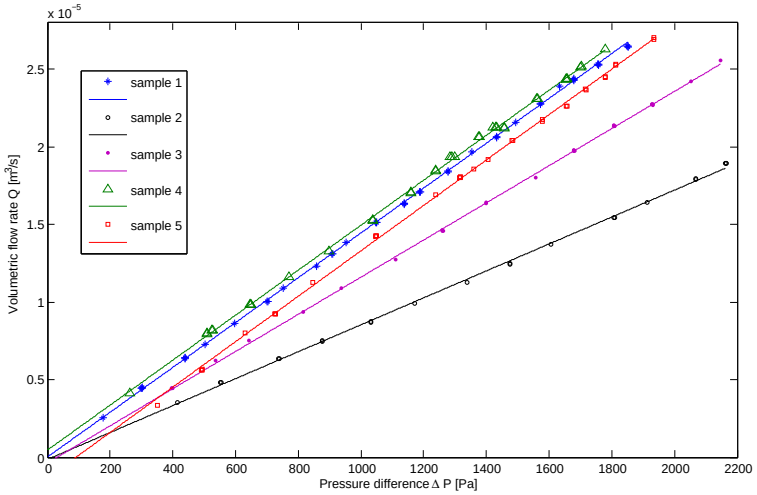

Figure 25: The pressure difference across the press felt sample as a function of water volume flow.